Detect Residential Buildings from Lidar and Aerial Photographs through Object-Oriented Land-Use Classification

Xuelian Meng, Nate Currit, Le Wang, and Xiaojun Yang

Abstract

Relating less directly to the physical reflectance from remote sensors, land-use analysis is comparably more challenging than land-cover studies, especially for residential land-uses. This research presents an object-oriented approach to detect residential land use of buildings directly from lidar data, aerial photography, and road maps to enhance urban land-use analysis. Specifically, the proposed methodology applies a multi-directional ground filter to generate a bare ground surface from lidar data, then uses a morphology-based building detection algorithm to identify buildings from lidar and aerial photographs, and finally separates residential buildings using a supervised C4.5 decision tree analysis based on seven land-use characteristics of buildings. Experiments based on the 8.25 km^2 study site located in Austin, Texas proved the possibility and efficiency of directly detecting and identifying residential buildings from remote sensing images with 81.1 percent of residential buildings correctly classified.

Introduction

Urban land-use analysis is critical in analyzing human-environment interactions. Many experiments have been conducted to classify built-up land, forest, water, and other land-use or land-cover types (Bruzzone and Carlin, 2006; Frate *et al.*, 2007; Houghton, 1994; Huang *et al.*, 2008). Separating residential land-uses from other uses within urban areas, however, has proven to be troublesome (Gong and Howarth, 1992; Herold *et al.*, 2003; Lu and Weng, 2006). Although high-resolution images have recently become more available for land-use classifications, an increasing spatial resolution does not guarantee improved performance of traditional classifiers due to the increase in class complexity (Barnsley *et al.*, 2001; Huang *et al.*, 2007; Martin *et al.*, 1988). Therefore, new approaches are needed that utilize the detailed texture information available in high-resolution imagery to improve urban land-use mapping.

Xuelian Meng is with the Department of Civil Engineering & Geodetic Science, The Ohio State University. Columbus, OH 43210, and formerly with Texas State University (meng.105@osu.edu).

Nate Currit is with the Geography Department, Texas State University-San Marcos, San Marcos, TX 78666.

Le Wang is with the Department of Geography, State University of New York at Buffalo, Wilkeson Quad, Buffalo, NY.

Xiaojun Yang is with the Department of Geography, Florida State University, Tallahassee, FL 32306.

Current urban land-use classification algorithms can be grouped into three categories: pixel-based, parcel-based, and object-oriented (Wu, 2006). Pixel-based methods classify individual pixels into land-use categories. Most pixel-based classification algorithms assume that the spectral distribution of each class is normal and perform poorly where this condition is not met. However, when image spatial resolution increases (e.g., from 30 meters to 1 meter), objects within a land-use type have unique colors and textures due to the variety of features visible at high resolution. As a result, a land-use category in high-resolution imagery more likely has a complex multi-modal spectral distribution, leading to statistical bias and inaccurate classification results (Herold *et al.*, 2003; Myint, 2003).

Incorporating neighborhood context into the pixel-based classification process, by including surrounding pixel values in a pre-defined neighborhood, provides a promising alternative. Barnsley and Barr (1996) utilized the Maximum Likelihood Classifier (MLC) to separate SPOT images into broad land-cover types and conducted a kernel-based spatial reclassification based on an adjacency matrix to reclassify the broader land-cover classes into the following land-use types: low and medium density residential, commercial/industry, arable crops, pasture, woodland, bare soil, and water. The results yielded a kappa coefficient of 0.92; however, no accuracy for individual residential land-use types was reported. Gong and Howarth (1992) applied a texture classification based on the frequency matrix and gray-level vector to classify 14 urban land-uses classes and improved the land-use classification from a kappa coefficient of 0.462 to 0.616. However, the window size for calculating neighborhood context has a significant influence on land-use classification accuracy (Gong and Howarth, 1992).

Researchers are exploring new approaches, notably parcel-based and object-oriented analyses, to solve the problems of pixel-based land-use classifications. An object in remote sensing imagery usually refers to an urban feature such as a building, roof top, parking lot or road. A parcel in land-use and land-cover classification is usually a space with a specified land-cover type or land-use function, which may contain mixed objects such as grass, road, and buildings. One common characteristic for many object-oriented classification methods is to focus on the detection of specific objects and collect object-associated characteristics for classification. Instead of classifying each individual pixel, parcel-based

Photogrammetric Engineering & Remote Sensing
Vol. 78, No. 1, January 2012, pp. 35–44.

0099-1112/12/7801–35/$3.00/0

land-use classifiers classify groups of pixels derived from existing GIS data or land-cover classification (Aplin *et al.*, 1999; Barnsley *et al.*, 2003; Bauer and Steinnocher, 2001; Zhan *et al.*, 2000). For example, Herold *et al.* (2003) first manually delineated land-cover parcels based on visual interpretation on Ikonos images and then applied the eCognition® software to incorporate spatial structure and texture information to classify land parcels into nine urban land-uses including four levels of residential land-use density. Bauer and Steinnocher (2001) conducted similar research based on the MLC-derived land-cover classes from Ikonos images. Pacifici *et al.* (2009) experimented with land-use classification based on high-resolution QuickBird and WorldView panchromatic images using a neural network and texture analysis. The results showed that applying neural network classification only on panchromatic images generate poor results (Kappa coefficient below 0.38), but that incorporating texture features with the panchromatic images significantly increased the accuracy (Kappa coefficient above 0.79). Applying an additional neural network to optimize and select the most distinguishable bands improved the kappa coefficient to be over 0.9. However, the accuracy for residential land uses was unknown. The accurate classification of residential land uses has proven to be difficult. Researchers often seek help from existing land-use or census maps (Wu *et al.*, 2006; Lu and Weng, 2006). Lu and Weng (2006) integrated impervious surface and census population density within a rule-based land-use classification system to classify the study site into urban non-residential land-use, non-urban, water, and residential land-uses with four density levels. Although the authors utilized census population data, the four residential land-uses were proven to be the most difficult to classify as the accuracies range from 54.55 percent to 82.46 percent with an average accuracy of 68 percent.

Object-oriented classifications detect and label objects that usually correspond to specific urban features (such as buildings, impervious surfaces, and others) and provide a different approach to simulate visual land-use interpretation logic. Targeting actual urban objects with the aid of adjacent features makes object-oriented classification similar to visual image interpretation. One advantage of this approach is that it is easier to assign statistics (e.g., area, perimeter, height, and distance to road) to objects (Huang and Zhang, 2008). However, relatively little object-oriented classification research has being done to date.

Instead of directly classifying land-uses based on buildings, some researchers select several study sites, each containing a single land-use type, to represent the variety of urban land-uses and to examine their characteristic differences based on selected properties associated with each land-use. Wu *et al.* (2006) selected two sets of test images for each of the five land-use characteristics of buildings (mobile home, single family, multi-family, commercial, and industry) and explored the response of land-use classification based on variogram analysis by alternating critical input parameters such as the window size and lag value. Similarly, Barr *et al.* (2004) selected several residential and industrial zones containing single land-use type, applied the graphical structural analysis software (SAMS) based on building vectors to examine the statistical characteristics of buildings such as area, compactness, node degree (number of edges to a node), and distance, and evaluated the land-use separability of buildings based on the Mann-Whitney U-test. A similar test was applied to a lidar-derived building map instead of the existing building data (Barnsley *et al.*, 2003) and accompanying land-cover vector data (Barnsley and Barr, 1997).

In this research, we explore the possibility of improving urban land-use classification by basing classifications on buildings and building-associated characteristics derived from remote sensing data and road maps. Specifically, this study aims to directly detect residential buildings from remote sensing date with a minimum support of GIS data, which requires three data sources: lidar data for building height, a road network map for distance to the major roads, and aerial photograph for the calculation of vegetation index. We propose an approach with three consecutive methods to detect buildings and building-associated characteristics and to identify residential buildings using an object-oriented supervised decision tree classifier. Due to the limitation of image-derived buildings, the residential buildings in this research refer to isolated buildings that are mainly used for residential purpose and may include apartment buildings, single-family or multi-family buildings, and their non-separable components. The expected deliverables are the distribution of residential buildings and the three-step approach for residential building detection. The following paper first introduces the study site and data collection, describes the three-step methodology, and then reports the experiment results.

Study Site and Data Collection

The study site is in a well-known population-growing city, Austin, Texas, where residential buildings may provide more clues for population distribution than the less-frequently updated census data. Austin is the Texas's fourth-largest city with a population of 709,893 according to the 2006 estimation (United State Census Bureau, 2009) and is the third fastest growing city in the nation based on censuses from 2000 to 2006 (Christie, 2007). The trend of rapid urbanization has increased in Austin with tremendous building development and change within and around the city. The 8.24 km^2 study site is located in the southern part of the city. Divided by the widest road in the middle, the left side of the image is dominated by downtown commercial buildings and the right side includes mainly residential buildings (Figure 1).

This research uses three data sources to develop and test a new approach to directly identify buildings and infer land-use information based on building-associated characteristics: (a) lidar data, (b) a 0.6 m (two-foot) resolution orthorectified digital aerial photography, and (c) a road map. The raw lidar data obtained in 2000 using the Optech ALTM lidar sensor contains three components: the first return, the last return, and intensity (City of Austin, 2009). The first return measures the laser backscatters from the surface of ground and objects. The last return measures the last backscatters from where

Figure 1. The grayscale image of the aerial photograph of the 8.24 km^2 study site in Austin, Texas.

laser beams can reach since laser beams can penetrate deeper in vegetation canopies. The lidar dataset has an average density of three points per square meter in this urban area. For this research, we first apply an outlier removal process based on Delaunay Triangulation to filter out random noises that may be backscatter from birds, airplanes or other objects and then transform the point clouds into a 1 m resolution raster data by assigning the elevation of the nearest point found within a specified distance of the pixel. No-data value is assigned when no points are found within the specified distance (Meng *et al.* 2009b; Meng, 2005).

The original aerial photograph was collected in 2000 with three visible bands and a near-infrared band (City of Austin, 2009). We interpolated the 0.6 m resolution photograph to one-meter resolution imagery to match the raster data derived from the lidar dataset and then calculated the standard Normalized Difference Vegetation Index (NDVI) based on red and near-infrared bands (Jensen, 2007). In this research, we manually generate a year-2000 road map by referencing the available 2003 road network file to the year-2000 aerial photograph and use the major road surfaces coded of 210 (edge of pavement) to calculate the distance from buildings to the nearest major road.

Detecting Residential Buildings from Lidar and Aerial Photographs

Residential building is an important statistic unit showing the spatial distribution of human population, which is critical for many human-driven environmental issues. In order to enable the identification of residential buildings from remote sensing imagery, it is necessary to detect buildings as objects and calculate their associated statistics to facilitate the statistical classification. Therefore, based on lidar data, aerial photographs, and road maps in this project, we developed a three-step approach as illustrated in Figure 2: the Multi-Directional Ground Filtering (MGF) for filtering ground from lidar data, a morphology-based building detection algorithm to detect buildings from the filtered non-ground areas of lidar data, and the object-oriented building land-use classification using seven characteristics and the supervised C4.5 algorithm. The technical details of the first two methods have been published in Meng *et al.* (2009a and 2009b). In this paper, we give a general introduction of the first two methods for a complete theoretical structure and then focus on the illustration of the third part in the following content.

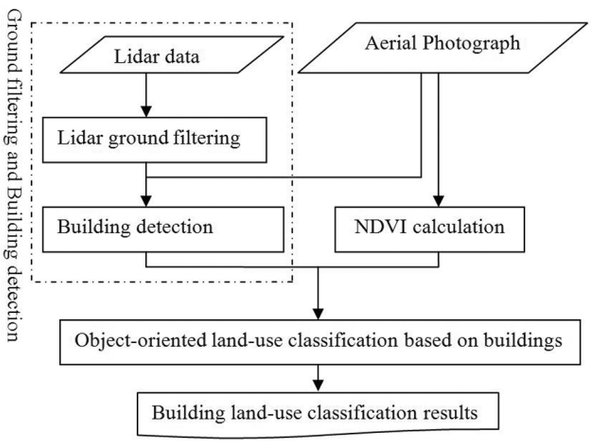

Figure 2. Conceptual design of the building-based object-oriented land-use classification.

Multi-Directional Ground Filtering

The abrupt changes of elevation and slope on the edge of trees, buildings, and other above-ground objects are usually different with those changes between adjacent ground locations (Meng *et al.*, 2010); hence we developed the Multi-Directional Ground Filtering (MGF) algorithm to separate ground area based on thresholds of slope and elevation difference calculated from the imagery interpolated using lidar data (Meng *et al.*, 2009b). The MGF algorithm has been previously tested on fifteen urban and rural sites provided by the International Society for Photogrammetry and Remote Sensing (ISPRS) and proven to be the second best overall and the best performing algorithm for three study sites after comparing to eight other methods (Meng *et al.*, 2009b; Sithole and Vosselman, 2004). We found that the MGF algorithm was robust to two commonly required parameters: slope and elevation difference which operated especially well in urban environments. Therefore, this research selects the MGF algorithm to filter the ground surface and generate a Digital Elevation Model (DEM).

The MGF algorithm separates ground from lidar data based on the elevation difference to the local minimum elevation and the nearest ground-labeled location, the ground or non-ground label of the previous location along a filtering direction, and slope. The algorithm repeats this labeling process from different filtering directions (left to right, right to left, top to bottom, and bottom to top) to gradually remove non-ground areas. Our previous study recommends a three-by-three search window for the search of local minimum elevation because increasing the search window usually decreases the ground filtering accuracy (Meng, 2005). In addition, our results indicated that the MGF algorithm is robust to the selection of scanning directions and any combination of three or four filtering directions will generate similar results (Meng, 2005). Therefore, there are usually two main parameters, slope and elevation difference, that need to be adjusted when testing for optimal results, and the remaining filtering process is automatic.

Morphology-Based Building Detection

After ground filtering and DEM generation, we apply a modified morphology-based building detection method to separate buildings from non-buildings. Meng *et al.* (2009a) developed the original method to extract buildings from lidar without the aid of aerial photographs to reduce the cost for its applications. Since aerial photographs are required in the followed classification step in this project, an improved version with NDVI data derived from a four-band digital aerial image integrated into the morphology-based building detection algorithm is used to facilitate the removal of dense trees and to improve the accuracy of the building detection.

The morphology-based building detection method gradually removes non-building objects based on various size and shape characteristics. After the ground filtering process, the remaining pixels at the Austin site are mainly composed of vegetation, buildings, and other objects, such as short walls and vehicles. Buildings differ from other objects in size, shape, height, and texture and can be separated using an analytical approach as illustrated in Figure 3. Laser light beams can penetrate vegetation areas and produce multiple returns of signals; hence areas with larger elevation differences between the first and last returns usually indicate vegetation and can be removed from the building candidates. The elevation difference between the lidar first return and the lidar-derived DEM represents height of the above-ground objects. Objects that are lower than the minimum building height can be removed from buildings. Similarly, areas or pixels with high NDVI indexes (calculated

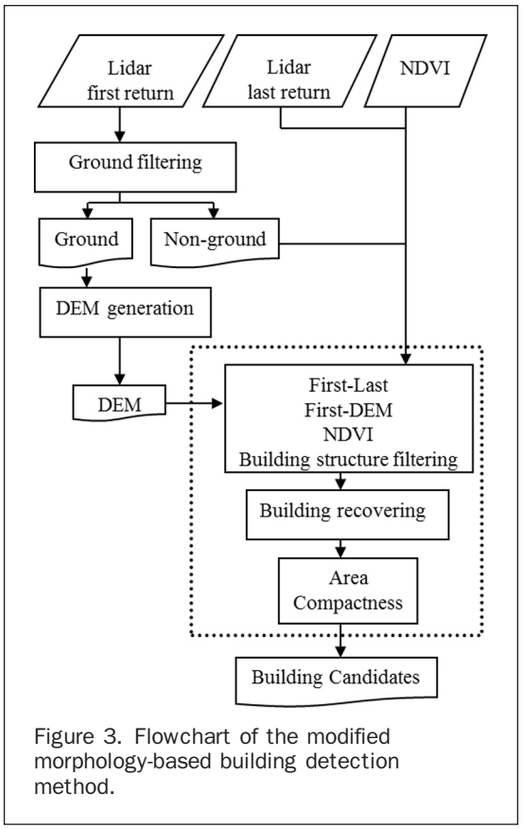

Figure 3. Flowchart of the modified morphology-based building detection method.

from the aerial photographs) indicate vegetated areas and should be removed. To this step, many remaining vegetated areas are in fragmented and narrow linear shapes while buildings are usually larger blocks of pixels. Therefore, the building detection method performs a building structure filtering process based on possible building pixel alignments within a three-by-three neighborhood to break non-building blocks into smaller fragments. A building recovery process then refills holes in buildings for pixels wrongly removed in the previous process. Finally, we convert building candidates into vectors, and then an object-oriented analysis further removes non-building parcels with area and compactness thresholds. Building compactness can be calculated through Equation 1 (Barnsley *et al.*, 2003). More detailed introduction for the morphology-based building detection can be found in Meng *et al.* (2009a).

$$\text{Compactness} = \text{area} \times \text{perimeter}^2/(4\Pi). \quad (1)$$

Object-Oriented Building Urban Land-Use Classification

Building areas on imagery belong to one of the land-cover types and may be separated based on reflectance characteristics; however the land-use characteristics of buildings such as residential, commercial, and industrial use are hard to separate using physical reflectance. This paper introduces an object-oriented classification method to separate buildings for residential use based on seven statistics associated with buildings. Identifying land-use characteristics from the buildings derived from remote sensing data involves three steps: selecting land-use characteristics associated with buildings, calculating land-use indicative statistics, and performing the land-use classification. Trained image interpreters can visually identify land-use functions of buildings utilizing certain context analyses, which include color, size, shape, texture, green space, parking space, the distance to roads, and others. The human vision system has the ability to naturally group image features as objects and identify land-uses based on a complex decision making system; however, a human designed automated system may not be able to easily identify those characteristics or other ancillary information (Quackenbush, 2004). An alternative approach is to learn from the human visual identification process and simplify the process to make it feasible for automated simulation.

Single-family residential, multi-family residential and other buildings usually have some common characteristics in developed countries (Barnsley *et al.*, 2003; Jensen, 2007). Important characteristics of residential and other buildings in developed countries are listed in Table 1 (Barnsley *et al.*, 2003; Herold *et al.*, 2003; Jensen, 2007). Because not every characteristic is detectable directly from remote sensing data or available from existing GIS data, we simplify characteristics from Table 1 and list in Table 2 the elements and land-use indicative characteristics that are detectable from remote sensing imagery or ancillary data sources. For example, green spaces, such as grass and trees, often surround residential buildings. Parking lots or concrete surfaces tend to be found surrounding commercial or industrial buildings compared to residential buildings. Additionally, commercial buildings are usually relatively closer to major roads so as to reduce the cost of transportation and attract customers. Because land-use characteristics differ from region to region and from developed to developing countries, it is important to understand the characteristics that identify local building types and incorporate them into the residential building classification process.

We then design seven statistics associated with each building as illustrated in Figure 4 based on detectable characteristics in Table 2 and use the statistics to classify residential and other buildings. These seven statistics include three building-based characteristics that were calculated in the building detection process: (a) area, (b) height, and (c) compactness. The other four statistics are based on the building's spatial context and adjacency relationships, including (d) the shortest distance to the major roads, (e) the percentage of green space within a buffer distance of existing buildings, (f) the percentage of parking spaces within a buffer distance of existing buildings, and (g) the building density in a street block. Statistics d to g can be calculated using GIS spatial analysis and zonal statistics tools as demonstrated in Figure 4. For the distance to the major road, we extract the major-road polygons based on the code in road data, use the distance function to generate a distance-to-road raster file, and finally calculate the shortest distance to road from each building using the zonal statistics of smallest distance values within a buffer zone of a building. Green space can be derived from the vegetation index of NDVI calculation using green and red bands from the aerial photograph and separated through a threshold (Jensen, 2007). Potential parking space is derived from the filtered ground area after further removing road and green space. Then, similar zonal statistic methods are applied to calculate the percentage of green and parking spaces within a buffer of buildings. The definition of block building density in this research is calculated by dividing the number of buildings within a block by the area of the block, where a block is defined as the polygons surrounded by streets in the road map (not the census block data). However, users can replace the street blocks using census block data if applicable.

We separate residential buildings by using the seven building-associated statistics as inputs to the C4.5 decision tree classifier. This research selects the C4.5 decision tree

TABLE 1. CHARACTERISTICS OF DIFFERENT BUILDING LAND-USE TYPES IN DEVELOPED COUNTRIES

Single-family residential	Single-family house	• A single driveway, distance to major roads • One front sidewalk leading to the front door • A front yard , a backyard (often fenced) • A garage or car port, Roof types, Size • Usually ⩽3 stories in height. • Space between houses, building density
	Small Mobile-home	• Much smaller than other single-family homes • Rarely have a garage (but may have a carport) • May have a paved driveway or sidewalk. • Roofs can be flat or pitched
Multi-family residential	Multi-family residential	• Large collective above- or below-ground parking garages, parking lots, or concrete ground covers • May be ⩾2 stories in height • Share front or back yards, Some have fences • Green spaces, outside swimming pools • Recreation courts • Similar building shape and size • More than one sidewalk • Some are in residential areas and are usually surrounded by residential buildings • Distance to major roads
Non-residential	Large	• Large building sizes • Next to large or small non-residential buildings • Along major roads • Huge open parking spaces in rural areas • High-rise buildings in downtown • May have multiple AC units
	Smaller	• Size may equal or larger than single-family house • Some storage or equipment room maybe smaller • Along major roads or at intersections • Next to non-residential buildings • Shared parking lots or no parking lots in downtown

TABLE 2. ELEMENTS AND LAND-USE INDICATIVE CHARACTERISTICS THAT CAN BE DERIVED FROM THE THREE DATA SOURCES: LIDAR, AERIAL PHOTOGRAPHS AND ROAD MAPS

Target elements	Source	Land-use indicative characteristics
Buildings	Detected*	Height, area, roof type, distance to the closest building, census block building density and building size diversity within a block
Green spaces	Detected	Size: small, middle, and large grass or trees
Water bodies	Detected	Size, shape
Parking lots or concrete ground covers	Detected	Size, area
Roads	GIS data	Classified roads from GIS data, two or three classes

*"Detected" means that the elements need to be generated or extracted from the three data resources.

classifier, which is used in a variety of land classification applications (Rogan *et al.*, 2008; Homer *et al.*, 2004; Friedl *et al.*, 1999). The C4.5 decision tree classifier was first introduced in computer science utilizing information theory to automatically generate splitting nodes for decision tree analysis (Quinlan, 1993). The algorithm uses the gain ratio as in Equation 2 to determine splitting thresholds:

$$\text{gain ratio}(X) = \text{gain}(X)/\text{split info}(X) \quad (2)$$

where gain (X) is the measurement of information entropy loss when attribute X is chosen for the test to divide and split info(X) measures the estimated information generated after assigning training samples to *n* classes. For algorithm details, see Quinlan (1993). The attribute X are the seven statistics in this research. The output of the C4.5 algorithm is a set of rules for distinguishing residential and other buildings and classified results.

Austin Site Verification

We design this object-oriented land-use classification method to directly detect residential buildings from remote sensing data and road maps. A proper verification process is necessary to adapt this method to local environment for the selection of parameters. In this research, the verification processes involve three procedures corresponding to ground filtering, building detection and land-use classification.

For the ground filtering process, our previous research tested the multi-directional ground filtering process on the fifteen study sites provided by ISPRS website and indicated that the algrithm is robust to parameter selection (Meng *et al.*, 2009b). The MGF algrithm was further validated on a local site of 0.016 km^2 in Austin using the same data source with this research (Meng, 2005). We select the ground filtering parameters when the algorithm achieves the highest accuracy based on a ground truth data generated by manual editing referencing to segmentation and a field survey on

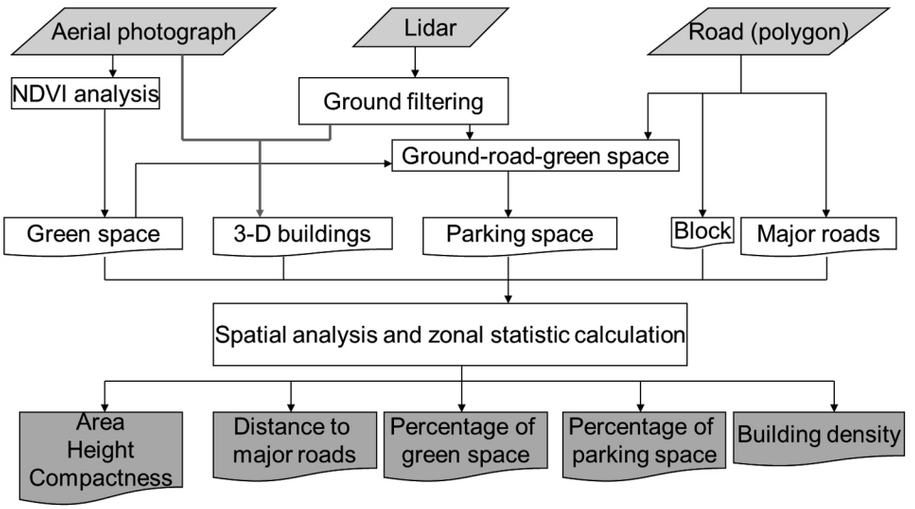

Figure 4. Flowchart showing the process to calculate the seven statistics from the three data sources using spatial analysis and zonal statistic tools.

07 May 2005. In this research, we then apply similar parameterss to the 8.24 km^2 study site with slight adjustment based on visual inspection of troublesome areas.

For the building detection verification, we validated the morphology-based building detection on a 0.67 km^2 Austin site using the same lidar source (Meng *et al.*, 2009b) and evaluated the building detection performance based on a building map verified through a field trip in 2007. We then applied the NDVI-integrated method as in Figure 3 to the bigger study site. Same parameters are applied for the building detection of the larger site in this research except a smaller compactness threshold because of the large residential area with smaller residential buildings on the right part. In addition, this research uses NDVI from aerial photography to reduce the confusion between large patchs of vegitation and buildings, especially when trees share boundaries with building rooves. For the NDVI shreshold, Barnsley *et al.* (2003) showed that 0.24 was efficient to separate vegetation from non-vegetation area. More detailed vegetation classification based on NDVI showed that areas with values around 0.21 may be dry grass (Etzelmüller *et al.*, 2006). Considering the dry weather in Texas, this research select 0.2 as NDVI threshold to separate vegetation for green space.

Spatial statistic calculation and classification accuracy evaluation are the major procedure for validation of the building-based land-use classification. When calculating statistics, we applied the road polygon from the City of Austin to extract major roads and blocks. Major roads were used to calculate the distance from buildings to the nearest major roads. We calculated the percentage of ground parking spaces within a 10-meter buffer distance to each building based on the potential ground parking spaces after removing roads and vegetation from the lidar ground filtering results. Polygons surrounded by roads served as blocks to calculate building density in a block by dividing the number of buildings within a block by the area of the block. To calculate the area of greenness within a buffer distance, we calculated NDVI using the red and near-infrared bands of the multispectral image and applied a threshold of 0.2 to filter out green areas including trees and grass. Then we calculated the percentage of green space within a 10 m buffer distance to buildings. To assess the performance of the building-based land-use classification, we randomly selected training and testing sets from the lidar-derived building map and surveyed the land-use characteristics of buildings based on a field trip in December of 2008.

Results and Discussion

The proposed object-oriented approach contains three major steps based on three consecutive methods: ground filtering, building detection, and land-use classification. The first two methods are quantitatively evaluated in two smaller local sites in previous research (Meng, 2005; Meng *et al.*, 2009a) and similar parameters are applied to the 8.24 km^2 study site in this research (Figure 5a).

The MGF ground filtering algorithm produced an overall accuracy of over 97 percent in the 0.016 km^2 test site (Meng, 2005). In this research, the ground filtering process uses 30° for the maximum ground slope, 0.7 meters for the elevation difference, scanning directions from each cardinal direction, and a three-by-three search window for local minimum elevation. Figure 5b is the ground filtering results where lighter color stands for higher elevation. The algorithm successfully identified main ground area with no obvious mis-identification. A few discrete errors may scatter around the boundaries between ground and non-ground areas as indicated in our previous study (Meng, 2005), which is common for many ground filtering process. One source of this type of errors is the un-avoidable disagreement between the manually labeled ground pixel and the detected ground pixels when their elevation difference to adjacent ground is close to the minimum ground elevation threshold, especially on object boundaries. But, the MGF algorithm overall provides very reliable result in this research in such relatively flat urban areas.

For the building detection process, Meng *et al.* (2009a) applied the morphology-based building detection to a local site of 0.67 km^2 using lidar data and produced an accuracy of 95.46 percent. In this research, a NDVI-integrated building detection method in Figure 3 applied similar parameters to the site in Figure 1 using lidar data and an aerial photograph. Parameters used in this step include thresholds of 0.2 m for the elevation difference between the first and last return,

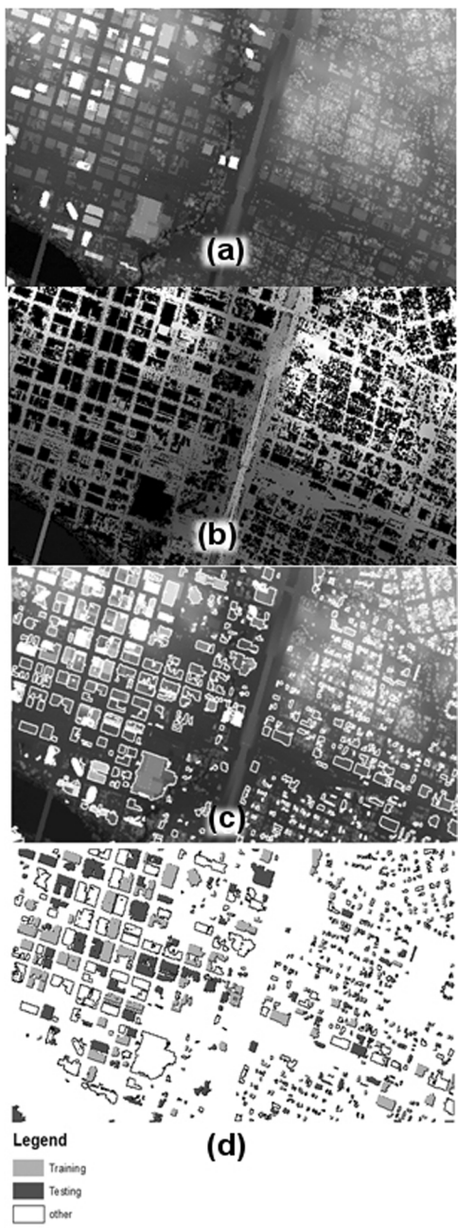

Figure 5. (a) Interpolated grayscale image of the lidar first return, (b) ground filtering results, (c) building detection result overlaid on interpolated image, and (d) training and testing sets for land-use classification.

2 m for the minimum building height threshold, 40 m^2 for the minimum building area, 12,000 for compactness, and 0.2 for NDVI index. Figure 5c is the results of final building candidates overlaid on top of interpolated imagery from the first return lidar data. The results show that this method successfully identifies buildings from the images. A few buildings, such as storage outbuildings, that are smaller than the minimum building threshold may be removed from the building candidates based on our previous study (Meng *et al.*, 2009a).

In the land-use classification process, we calculated the seven spatial statistics after deriving building footprints in the previous processes and applied a supervised land-use classification based on a randomly selected training and test dataset, whose land-use properties have been verified through a field survey. Table 3 lists the statistics of residential and non-residential buildings in both training and testing datasets, and Figure 5d shows their spatial distribution. The results of land-use survey reveal that a total of ten polygons of trees fail to be removed from the buildings: about 2.55 percent of the sampled building datasets. Few large areas of dense and tall trees that are comparable to the size and height of buildings (especially in residential areas in developed countries where many trees surround small residential houses) may remain in the building candidates if not covered by the vegetated areas from NDVI calculated from aerial photographs. The confusion between buildings and trees is a challenging problem for lidar-based building detection. Using both lidar and NDVI index from aerial photographs cannot guarantee the complete removal of trees due to few factors such as different tree crown coverage because of view angle in other aerial photographs, time difference in year or month, and tree cutting during the time difference. After running the C4.5 decision tree classification, this experiment reports 83.8 percent accuracy for correctly classified buildings, 81.1 percent accuracy for residential buildings, and 85.7 percent accuracy for other buildings. Table 4 shows the confusion matrix with statistics of buildings for residential and the other. Misclassified buildings include 14 residential buildings and 15 other types of buildings. Our field survey shows that several buildings with mixed or unusual land-uses may contribute to the misclassification, which include an old family-size coffee factory transformed from a residential building, a few three-level multi-residential buildings in downtown area, and a hotel-like building of multi-residential dorm for senior residence. In developing and undeveloped countries, lands with mixed residential and commercial uses are quite common, which can largely lead to the difficulty in separating land-uses through a building unit for both ground truth data and classification. Figure 6 illustrates the decision tree rules automatically generated by the C.45 classifier. The derived decision tree gives a higher priority to compactness, block building density, and building height and relatively a lower priority to greenness, distance to road, and parking. This is reasonable for the test site considering its location in an old urban-core area. Main streets are widely distributed in the entire site and the distance to major roads may be undistinguishable to separate residential and other buildings. In addition, less open parking spaces (garage parking cannot be detected as parking in this research) are available in old downtown area in the left side.

The main purpose of this research is to directly identify residential buildings from lidar and aerial photographs. We applied a three-step approach to first remove ground through a ground filtering process, identify buildings based on a morphological building detection, and then separate residential buildings through object-oriented land-use

TABLE 3. THE NUMBER AND PERCENTAGE OF BUILDING POLYGONS AND TREES USED IN THE TRAINING AND TESTING DATA

	Total building candidates		Buildings in training	Buildings in testing
Residential	169	43.11%	94	75
Non-residential	213	54.34%	109	104
Tree	10	2.55%		

TABLE 4. CONFUSION MATRIX FOR THE RESIDENTIAL AND NON-RESIDENTIAL LAND-USE CLASSIFICATION

		Reference		Classification accuracy
		Residential	Other	
Classified	Residential	60	14	81.1%
	Other	15	90	85.7%

classification based on spatial relationships between buildings and surrounding objects. Our test on the 8.24 km^2 Austin study site successfully detected over 81 percent of the residential buildings based on three data sources: lidar data, aerial photographs, and road maps.

Conclusions

Land-use classification is a challenging task in urban remote sensing, especially for residential land-uses. Residential land-uses relate closely to human activities and population distribution and have attracted a growing concern in urban land-use studies. Researchers have explored more pixel- and parcel-based approaches but little about object-oriented methods. Furthermore, ancillary land-use information or census population data are often necessary to improve urban land-use classification as land-use types relate less directly to physical reflectance of remote sensing imagery. Based on the lidar data, aerial photographs, and road maps in this research, we propose a three-step approach to directly detect buildings and separate residential buildings from remote sensing data: a multi-directional ground filtering (MGF) algorithm, a morphology-based building detection method, and an object-oriented land-use classification.

In the experiments based on sites in Austin, Texas, this research applied the MGF algorithm to separate ground from other features in lidar data and generate bare Earth DEM model, utilized the morphology-based building detection method to extract buildings from lidar data and aerial photographs, and then used an object-oriented building-based urban land-use classification approach to separate residential buildings.

In the building-based land-use classification process, we designed and calculated seven spatial statistics associated with buildings to characterize land-use types. The statistics are (a) building area, (b) height, (c) compactness, (d) the distance to major roads, (e) the area of green spaces within a

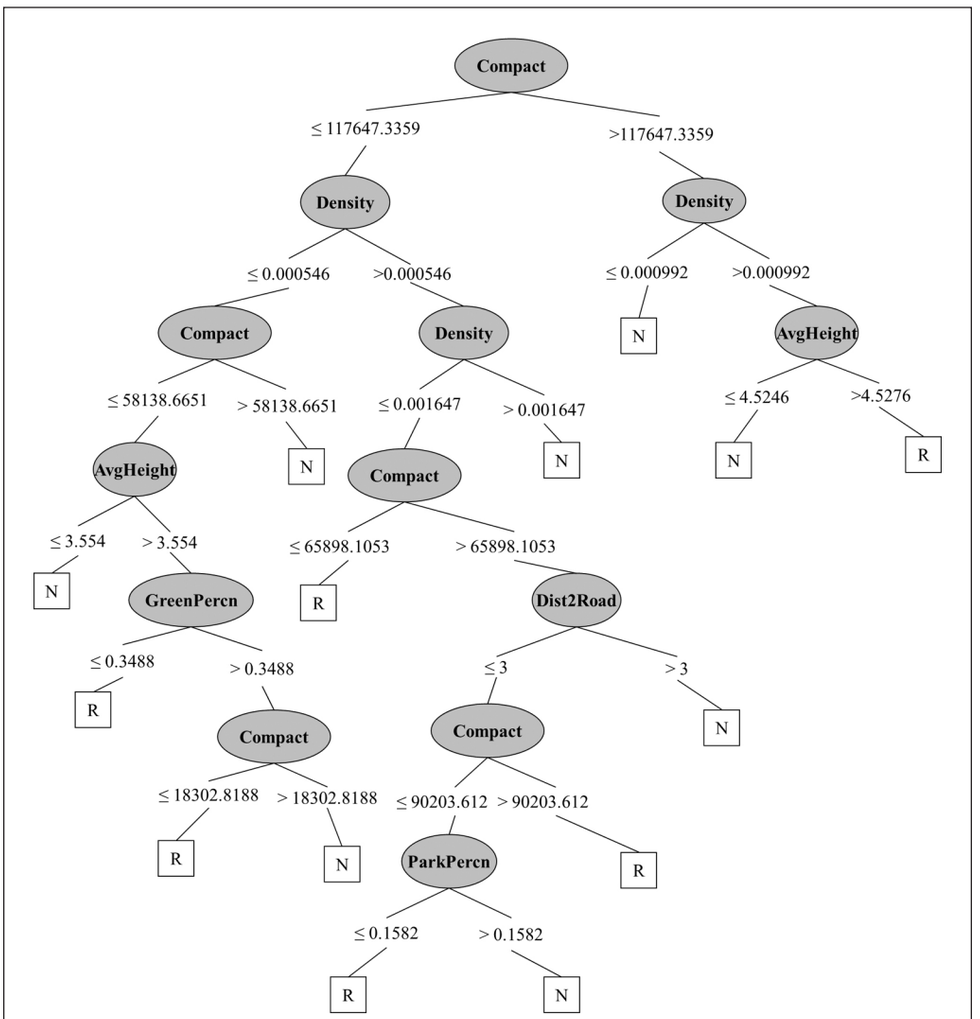

Figure 6. The decision tree rules automatically generated by the C 4.5 classifier dataset.

buffer distance, (f) the area of parking space within a buffer distance, and (g) the building density within a block. We then applied the supervised C4.5 decision tree classification method to separate residential and other buildings. Verification of results is based on randomly selected training and testing samples with land-uses collected through a field. Based on the experiment, around 2.55 percent of buildings failed to be removed during building detection due to the vegetation coverage difference caused by data source, time difference, and cut or plant of trees due to civil construction. The building-based classification method, however, successfully identified 81.1 percent of the residential buildings and 85.7 percent of other buildings. Few buildings with uncommon land-uses will contribute to the classification error such as the small family-size factory, multi-family buildings in commercial zones, and abandoned buildings.

The potential usage of the detected residential buildings includes distribution of resources, population estimation based on residential buildings to compensate the less-frequently updated census data, population estimation based on boundaries that are different with census statistic boundaries (such as flooded areas), site selection based on customer estimation, redistribution of census population based on residential buildings and height, and sub-block level population estimation. Furthermore, the experimented verification processes provide practically value to adapt these methods to local environment for large area DEM, building, and building-based land-use mapping for various applications.

Acknowledgments

This study was supported by grants to Le Wang from the National Science Foundation (BCS-0822489).

References

Aplin, P., P. Atkinson, and P. Curran, 1999. Fine spatial resolution simulated satellite sensor imagery for land cover mapping in the United Kingdom, *Remote Sensing of Environment*, 68(3):206–216.

Barnsley, M.J., and S.L. Barr, 1996. Inferring urban land-use from satellite sensor image using Kernel-based spatial reclassification, *Photogrammetric Engineering & Remote Sensing*, 62(8):949–958.

Barnsley, M.J., and S.L. Barr, 1997. Distinguishing urban land-use categories in fine spatial resolution land-cover data using a graph-based, structural pattern recognition system, *Computers, Environment and Urban Systems*, 21(3/4):209–225.

Barnsley, M.J., L. Møller-Jensen, and S.L. Barr, 2001. Inferring urban land-use by spatial and structural pattern recognition, *Remote Sensing and Urban Analysis* (J. Donnay, M.J. Barnsley, and P.A. Longley, editors), Taylor & Frances, London, pp. 115–144.

Barnsley, M.J., A.M. Steel, and S.L. Barr, 2003. Determining urban land-use through an analysis of the spatial composition of buildings identified in LIDAR and multispectral image data, *Remotely Sensed Cities* (V. Mesev, editor), Taylor & Frances, New York, pp. 83–108.

Barr, S., M.J. Barnsley, and A. Steel, 2004. On the separability of urban land-use categories in fine spatial scale land cover data using structural pattern recognition, *Environment and Planning B: Planning and Design,* 31:397–418.

Bauer, T., and K. Steinnocher, 2001. Per parcel land-use classification in urban areas applying a rule-based technique, *GeoBIT/GIS*, 6:24–27.

Bruzzone, L., and L. Carlin, 2006. A multilevel context-based system for classification of very high spatial resolution images, *IEEE Transactions on Geoscience and Remote Sensing*, 44(9):2587–2600.

Christie, L., 2007. *The Fastest Growing U.S. Cities*, CNNMoney.com, URL: *http://money.cnn.com/2007/06/27/real_estate/fastest_growing_cities/* (last date accessed: 27 September 2011).

City of Austin, 2009. *Austin, Texas: Basic Facts*, URL: *http://www.ci.austin.tx.us/citymgr/ basicfac.htm* (last date accessed: 05 April 2009).

Etzelmüller, B., E.S. Flo Heggem, N. Sharkhuu, R. Frauenfelder, A. Kääb, and C. Goulden, 2006. Mountain permafrost distribution modelling using a multi-criteria approach in the Hövsgöl Area, Northern Mongolia, *Permafrost and Periglacial Processes*, 17(2):91–104.

Frate, F.D., F. Pacifici, G. Schiavon, and C. Solimini, 2007. Use of neural networks for Automatic classification from high-resolution images, *IEEE Transactions on Geoscience and Remote Sensing*, 45(4):800–809.

Friedl, M.A., C.E. Brodley, and A.H. Strahler, 1999. Maximizing land-cover classification accuracies produced by decision trees at continental to global scales, *IEEE Transactions on Geoscience and Remote Sensing*, 37(2):969–977.

Gong, P., and P.J. Howarth, 1992. Frequency-based contextual classification and gray-level vector reduction for land-use identification, *Photogrammetric Engineering & Remote Sensing*, 58(4):423–437.

Herold, M., X. Liu, and K. Clarke, 2003. Spatial metrics and image texture for mapping urban land-use, *Photogrammetric Engineering & Remote Sensing*, 69(6):991–1001.

Homer, C., C. Huang, L. Yang, B. Wylie, and M. Coan, 2004. Development of a 2001 National Land-Cover Database for the United States, *Photogrammetric Engineering & Remote Sensing*, 70(3):829–840.

Houghton, R.A, 1994. The worldwide extent of land-use change, *Bioscience*, 44(5):305–313.

Huang, X., L. Zhang, and P, Li, 2007. Classification and extraction of spatial features in urban areas using high-resolution multispectral imagery, *IEEE Geoscience and Remote Sensing Letters*, 4(2):260–264.

Huang, X., and L. Zhang, 2008. An adaptive mean-shift analysis approach for object extraction and classification from urban hyperspectral imagery, *IEEE Transactions on Geoscience and Remote Sensing*, 46(12):4173–4185.

Huang, X., L. Zhang, and P. Li, 2008. Classification of very high spatial resolution imagery based on the fusion of edge and multispectral information, *Photogrammetric Engineering & Remote Sensing*, 74(12):1585–1596.

Jensen, J., 2007. *Remote Sensing of the Environment: An Earth Resource Perspective*, Prentice Hall, Saddle River, New Jersey.

Lu, D., and Q. Weng, 2006. Use of impervious surface in urban land-use Classification, *Remote Sensing of Environment*, 102:146–160.

Martin, L., P.J. Howarth, and G. Holder, 1988. Multispectral classification of land-use at the urban-rural fringe using SPOT satellite data, *Canadian Journal of Remote Sensing*, 14:72–79.

Meng, X., 2005. A slope- and elevation-based filter to remove non-ground measurements from airborne LIDAR data, *Proceedings of theUCGIS Summer Assembly*, 28 June-01 July, Jackson Hole, Wyoming.

Meng, X., L. Wang, N. Currit, 2009a. Morphology-based building detection from airborne lidar data, *Photogrammetric Engineering & Remote Sensing*, 75(4):427–442.

Meng, X., L. Wang, J.L. Silván-Cárdenas, N. Currit, 2009b. A multi-directional ground filtering algorithm for airborne LIDAR, *ISPRS Journal of Photogrammetry and Remote Sensing*, 64(1):117–124.

Meng, X., N. Currit, and K. Zhao, 2010. Ground filtering algorithms for airborne LiDAR data: A review of critical issues, *Remote Sensing*, 2(3):833–860.

Myint, S.W., 2003. The use of wavelets for feature extraction of cities from satellite sensor images, *Remotely Sensed Cities* (V. Mesey, editor), Taylor & Frances, New York, pp. 109–134.

Pacifici, F., M. Chini, and W.J. Emery, 2009. A neural network approach using multi-scale textural metrics from very high-resolution panchromatic imagery for urban land use classification, *Remote Sensing of Environment,* 113:1276–1292.

Quackenbush, L.J., 2004. A review of techniques for extracting linear features from Imagery, *Photogrammetric Engineering & Remote Sensing,* 70(12):1383–1392.

Quinlan, J.R., 1993. *C4.5: Programs for Machine Learning*, Morgan Kaufmann Publishers.

Rogan, J., J. Franklin, D. Stow, J. Miller, C. Woodcock, and D. Roberts. 2008. Mapping Land cover modifications over large areas: A comparison of machine learning Algorithms, *Remote Sensing of Environment,* 112(5):2272–2283.

Sithole, G., and G. Vosselman, 2004. Experimental comparison of filter algorithms for bare earth extraction from airborne laser scanning point clouds, *ISPRS Journal of Photogrammetry and Remote Sensing*, 59(1-2):85–101.

United States Census Bureau, 2009. *States & County Quickfacts*, URL: *http://quickfacts.census.gov/qfd/states/48/4805000.html* (last date accessed: 27 September 2011).

Wu, S., 2006. *Incorporating GIS and Remote Sensing for Census Population Desegregation*, PhD Dissertation, Texas State University-San Marcos, 130 p.

Wu, S., B. Xu, and L. Wang, 2006. Urban land-use classification using variogram-based analysis with an aerial photograph, *Photogrammetric Engineering & Remote Sensing*, 72(7):813–822.

Zhan, Q., M. Molenaar, and B. Gorte, 2000. Urban land-use classes with fuzzy membership and classification based on integration of remote sensing and GIS, *International Archives of Photogrammetry and Remote Sensing*, 33:1751–1759.

(Received 04 May 2010; accepted 27 January 2011; final version 23 June 2011)